The 8th European Congress on Computational Methods in Applied Sciences and Engineering
ECCOMAS Congress 2022
5-–9 June 2022, Oslo, Norway

ON THE ALGEBRAIC MODIFICATIONS OF TRADITIONAL TURBULENCE MODELS TO PREDICT BYPASS AND SEPARATION-INDUCED TRANSITION

ALESSANDRO COLOMBO[1], ANDREA CRIVELLINI[2], ANTONIO GHIDONI[3], ALESSANDRA NIGRO[2] AND GIANMARIA NOVENTA[3]

[1] University of Bergamo,
Department of Engineering and Applied Sciences,
Viale Marconi 5, 24044 Dalmine (BG), Italy
e-mail: alessandro.colombo@unibg.it

[2] Marche Polytechnic University,
Department of Industrial Engineering and Mathematical Science,
via Brecce Bianche 12, 60131, Ancona, Italy
email: a.crivellini@staff.univpm.it, a.nigro@staff.univpm.it

[3] University of Brescia,
Department of Mechanical and Industrial Engineering,
via Branze 36, 25123 Brescia, Italy
email: antonio.ghidoni@unibs.it, gianmaria.noventa@unibs.it

Key words: discontinuous Galerkin, RANS equations, transition models

Abstract. Many reliable and robust turbulence models are nowadays available for the Reynolds-Averaged Navier-Stokes (RANS) equations to accurately simulate a wide range of engineering flows. However, turbulence models are not able to correctly predict flow phenomena with low to moderate Reynolds numbers, which are characterized by strong transitions. Laminar to turbulent transition is common in aerospace, turbomachinery, maritime, and automotive. Therefore, numerical models able to accurately predict transitional flows are mandatory to overcome the limits of turbulence models for the efficient design of many industrial applications. A modified version of the k-$\tilde{\omega}$ and Spalart-Allmaras turbulence models is proposed in order to predict transition due to the bypass and separation-induced modes. The modifications here proposed are based on the γk-ω and the SA-BCM transition models. Both the models are correlation-based algebraic transition models that relies on local flow information and include an intermittency function instead of an intermittency equation. The basic idea behind the models is that, instead of writing a transport equation for intermittency, an intermittency function multiplies the production terms of the turbulent working variables of the formulation of the turbulence models. In particular, the turbulence production is damped until it satisfies some transition onset requirements. The proposed models are implemented in a high-order discontinuous Galerkin (dG) solver and validated on different transitional benchmark cases from the ERCOFTAC T3 suite, with bypass (T3A, T3A- and T3B) and separation-induced (T3L1 and T3L3) transition.

1 INTRODUCTION

Literature classifies transition models into non-local and local models [3, 4]. The non-local models are based on correlations and the main drawback is due to the fact that needs the information on the integral thickness of the boundary layer and the state of the flow at the edge of the boundary layer. While the local models are based on transport equations for turbulent or transitional variables, similarly to the classical turbulence model, and require only local variables. The local formulation guarantees better robustness, accuracy and easiness of implementation in modern solvers. These models can be divided into correlation-based and phenomenological transition models.

Transition models have been meanly proposed for finite volume methods (FVM) to predict the laminar-turbulent transition, but the increasing required level of resolution naturally leads to consider discretization methods with a higher order of accuracy, such as the discontinuous Galerkin (dG) methods. In dG methods the solution of the weak or variational form of a partial differential problem is approximated by polynomial functions over the elements, similarly to the classical continuous finite element method (FEM). However, unlike continuous finite element methods, dG methods use an approximation that is in general discontinuous at the element interfaces. The coupling of the approximate solutions between neighboring elements is (weakly) enforced by interface, or numerical, fluxes. An appropriate definition of numerical flux guarantees the consistency and stability of the dG numerical approximation. The main drawback of this higher accuracy is the increased computational cost compared to standard FVM, but the compact stencil of dG spatial approximation, involving only one element and its neighbours, makes the method very well suited for massively parallel computer platforms. Furthermore, the computational efficiency of dG solvers can be substantially improved by resorting to multilevel solution approaches, such as the p-multigrid algorithms [11].

A modified version of the k-$\tilde{\omega}$ [8] and Spalart-Allmaras [10] turbulence models is here proposed and implemented in a high-order dG solver, called MIGALE, in order to predict transition due to the bypass and separation-induced modes. The modifications are based on the γk-ω by Holman and Fürst [7] and Kubacki et al. [13], and the SA-BCM by Cakmakcioglu et al. [9]. Both the models are correlation-based algebraic transition models that relies on local flow information and include an intermittency function instead of an intermittency equation. The basic idea behind the models is that, instead of writing a transport equation for intermittency, an intermittency function multiplies the production terms of the classical formulation of the turbulence models.

The choice of the transition models falls in the fact that the starting turbulence models, i.e., the k-$\tilde{\omega}$ and Spalart-Allmaras models, are yet implemented and widely assessed in the MIGALE solver (see Fig. 1). Where, the main goal of this work is to develop an easy modification of traditional turbulence models in order to predict transition, i.e., to write transition models without the adding of transport equations or the full rewriting of the production and dissipation terms of the turbulent working variables.

The prediction capabilities of these transition models are proved and assessed by computing the flow over the flat plates of the ERCOFTAC T3 series with zero pressure gradients, investigated experimentally by Coupland [6]. These test cases are mainly characterized by bypass and separation-induced transition, with different Reynolds number and freestream turbulent intensity. In particular in the ERCOFTAC zero pressure gradient flat plats, e.g., T3A, T3B and

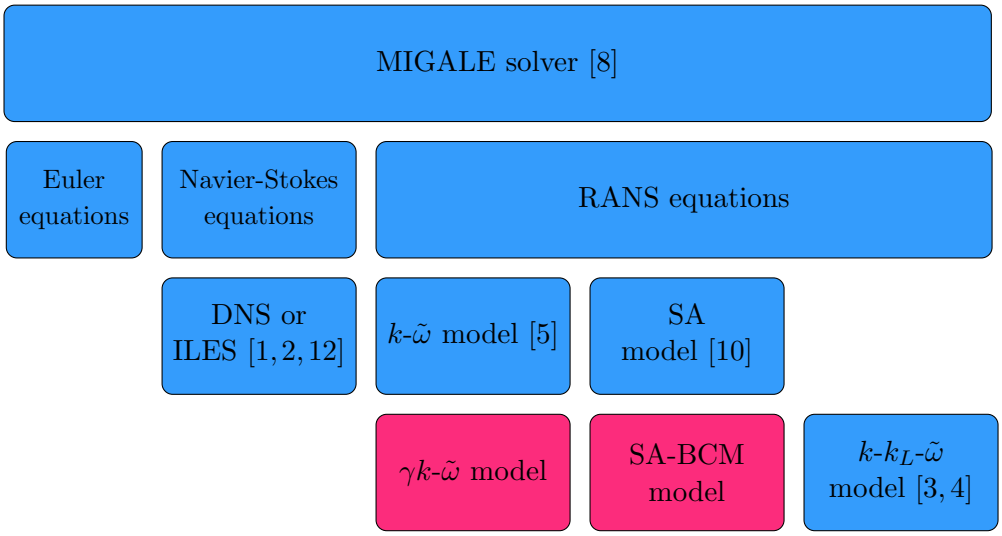

Figure 1: Representative scheme of the MIGALE solver, where compressible and incompressible Euler, Navier-Stokes and RANS equations are discretized and solved in an high-order spatial and temporal dG framework. Below the RANS equations box the first line of boxes represents the turbulence models, while the second line the transition models. The red boxes spotlight the transition models here proposed, as a further development of the k-$\tilde{\omega}$ and Spalart-Allamaras turbulence models

T3A- cases, the transition is in the bypass mode, while in the ERCOFTAC rounded leading edge flat plates, e.g., T3L1 and T3L3 cases, the transition is in the separation-induced mode. Where in the latter cases the separation is due to the geometry and only the reattachment has to be triggered by the model. This testsuite proves the well behaviour of the proposed transition models, in terms of the skin friction coefficient distribution on the wall in comparison with experiments and numerical results from literature [7, 15].

2 SA-BCM MODEL

The incompressible Spalart-Allmaras BCM transition model [9] equation can be written as

$$\frac{\partial \tilde{\nu}}{\partial t} + \frac{\partial}{\partial x_j}\left(u_j \tilde{\nu}\right) = \gamma_{BC} c_{b1} \tilde{S} \tilde{\nu} - c_{w1} f_w \left(\frac{\tilde{\nu}}{d}\right)^2 + \frac{1}{\sigma}\left[\frac{\partial}{\partial x_j}\left(\left(\nu + \tilde{\nu}\right)\frac{\partial \tilde{\nu}}{\partial x_j}\right) + c_{b2}\frac{\partial \tilde{\nu}}{\partial x_j}\frac{\partial \tilde{\nu}}{\partial x_j}\right]$$

where the density is a constant and $p^* = p/\rho$, $\widehat{\tau}^*_{ji} = \widehat{\tau}_{ji}/\rho$, and $\tau^*_{ji} = \tau_{ji}/\rho$. The turbulent viscosity and the closure functions are given by

$$\nu_t = \max\left(0, \tilde{\nu}\right) f_{v1}, \qquad f_{v1} = \frac{\chi^3}{\chi^3 + c_{v1}^3}, \qquad \chi = \frac{\tilde{\nu}}{\nu},$$

$$\tilde{S} = \Omega + \frac{\tilde{\nu}}{\kappa^2 d^2} f_{v2}, \qquad f_{v2} = 1 - \frac{\chi}{1 + \chi f_{v1}},$$

$$f_w = g\left[\frac{1 + c_{w3}^6}{g^6 + c_{w3}^6}\right]^{1/6}, \qquad g = r + c_{w2LRe}\left(r^6 - r\right), \qquad r^* = \frac{\tilde{\nu}}{\tilde{S}\kappa^2 d^2}.$$

where $\tilde{\nu}$ is kept non negative in the turbulent viscosity. The equation for r^* represents the standard definition of the r closure function which is modified according to

$$r = \begin{cases} \max(r^*, r_{max}) & r^* < 0 \\ \min(r^*, r_{max}) & r^* \geq 0 \end{cases}. \tag{1}$$

This approach, which avoids the sign inversion of the source terms, greatly improves the stability of the solution procedure, particularly in a high-order solver [10]. The intermittency function γ_{BC} is defined as

$$\gamma_{BC} = 1 - \exp\left(-\sqrt{Term_1} - \sqrt{Term_2}\right), \tag{2}$$

with two different functions, e.g., the $Term_1$ and $Term_2$, defined as

$$Term_1 = \frac{\max\left(Re_\theta - Re_{\theta c}, 0\right)}{\chi_1 Re_{\theta c}}, \qquad Term_2 = \max\left(\frac{\nu_t}{\chi_2 \nu}, 0\right), \tag{3}$$

where $Re_\theta = Re_{d^2\Omega}/2.193$ is the momentum thickness Reynolds number and $Re_{d^2\Omega} = d^2\Omega/\nu$ is the vorticity Reynolds number. The threshold value $Re_{\theta c}$ is a critical momentum thickness Reynolds number, which is written with a formulation based on experiments, i.e., $Re_{\theta c} = 803.73\left(Tu_\infty + 0.6067\right)^{-1.027}$. $Term_1$ is mainly responsible for the production of the intermittency function, in fact starts the production which is supported downstream by the $Term_2$. Where $Term_1$ is not able to generate intermittency inside the boundary layer, and $Term_2$ has been added recently [9] to overcome this limitation. The transition model constants are tabulated in Tab. 1. The model constant c_{w2} is replaced by c_{w2LRe} according to Spalart and Garbaruk [16], defined as

$$c_{w2LRe} = c_{w4} + \frac{c_{w5}}{\left(\frac{\chi}{40} + 1\right)^2},$$

to introduce the dependence from the turbulence model working variable χ. In the original model [9] the inlet or freestream working variable $\tilde{\nu}_\infty$ is set from 0.015ν to 0.025ν. Notice that the influence of the freestream turbulent intensity Tu_∞ is taken into account through $Re_{\theta c}$, and not by the working variable $\tilde{\nu}_\infty/\nu$. Finally, the standard $\tilde{\nu}_{wall} = 0$ condition is used at the wall boundaries.

3 γk-$\tilde{\omega}$ MODEL

The compressible γk-$\tilde{\omega}$ transition model equations can be written as

$$\begin{aligned}
&\frac{\partial}{\partial t}(\rho k) + \frac{\partial}{\partial x_j}(\rho u_j k) = \frac{\partial}{\partial x_j}\left[(\mu + \sigma^* \overline{\mu}_t)\frac{\partial k}{\partial x_j}\right] + \gamma_i f_W f_{SS} f_\nu C_\mu \tau_{ij}\frac{\partial u_i}{\partial x_j} + \\
&\qquad + \max\left[(1-\gamma_i)\max\left(2.8 Tu_\infty \mu - \overline{\mu}_t, 0\right) C_{SI} F_{SI} S^2, C_{Kleb} f_{Kleb} k S\right] - \beta^* \rho \overline{k} e^{\widetilde{\omega}_r}, \\
&\frac{\partial}{\partial t}(\rho \widetilde{\omega}) + \frac{\partial}{\partial x_j}(\rho u_j \widetilde{\omega}) = \frac{\partial}{\partial x_j}\left[(\mu + \sigma \overline{\mu}_T)\frac{\partial \widetilde{\omega}}{\partial x_j}\right] + \gamma_i f_W f_{SS} f_\nu C_\mu \frac{\alpha}{\overline{k}} \tau_{ij}\frac{\partial u_i}{\partial x_j} + \\
&\qquad - \beta \rho e^{\widetilde{\omega}_r} + (\mu + \sigma \overline{\mu}_T)\frac{\partial \widetilde{\omega}}{\partial x_k}\frac{\partial \widetilde{\omega}}{\partial x_k},
\end{aligned}$$

Table 1: Constants of the γk-$\tilde{\omega}$ model (top) and of the SA-BCM model (bottom), where only the constants of the transitional model are here reported. While α, α^*, β, β^*, σ and σ^* are the constants of the original k-$\tilde{\omega}$ model [8]

$A_0 = 4.04$	$A_S = 2.12$	$A_\nu = 5.20$
$A_{TH\,1} = 0.2$	$A_{TH\,2} = 0.2$	$A_{TH\,3} = 0.1$
$C_{TH\,1} = 21$	$C_{TH\,2} = 1.05$	$C_{TH\,3} = 0.002$
$C_S = 1.7$	$C_\lambda = 2.495$	$C_{INT} = 0.95$
$C_{\mu,std} = 0.09$	$C_k = 6$	$C_\chi = 10$
$A_{SI} = 1000$	$C_{SI} = 2$	$C_{Kleb} = 1/2$
$C_{Kleb,\gamma} = 2$	$b_\gamma = 150$	$a_\gamma = 0.95$
$a_\omega = 20$	$b_\omega = 5$	
$\chi_1 = 0.002$	$\chi_2 = 50$	
$\chi_1 = 0.002$	$\chi_2 = 50$	$r_{max} = 10^3$
$c_{b1} = 0.1355$	$c_{b2} = 0.622$	$\sigma = 2/3$
$c_{w1} = \frac{c_{b1}}{\kappa^2} + \frac{1+c_{b2}}{\sigma}$	$c_{w3} = 2$	$c_{w4} = 0.21$
$c_{w5} = 1.5$	$c_{v1} = 7.1$	$\kappa = 0.41$

where $\overline{\mu}_t = \alpha^* \rho \overline{k} e^{-\widetilde{\omega}_r}$ and $\overline{k} = \max(0, k)$. The transition model constants are tabulated in Tab. 1. The bypass transition prediction capabilities are represented by different damping functions, e.g., the shear-sheltering f_{SS}, the wall f_W and the viscous f_ν function, the turbulent viscosity coefficient C_μ and the intermittency function γ_i. In comparison with the original γk-ω model proposed by Kubacky et al. [13] and Holman and Fürst [7], where only the shear sheltering function is defined, here several damping functions are added according to the local and phenomenological k-k_L-$\tilde{\omega}$ transition model proposed by Lorini et al. [3, 4]. The kinematic wall effect is included through an effective wall-limited turbulent length scale λ_{eff} and the wall damping function f_W, as

$$\lambda_{eff} = \min\left(C_\lambda d, \lambda_T\right), \qquad f_W = \left(\frac{\lambda_{eff}}{\lambda_T}\right)^{\frac{2}{3}},$$

where $\lambda_T = \sqrt{k}/\omega$ is the turbulent length scale and d is the wall distance. The viscous wall effect is incorporated through a viscous damping function defined as

$$f_\nu = 1 - \exp\left(-\frac{\sqrt{Re_T}}{A_\nu}\right),$$

where $Re_T = f_W^2 k / \left(\nu e^{\tilde{\omega}}\right)$ is the effective turbulence Reynolds number. The turbulent viscosity coefficient takes the form

$$C_\mu = \frac{1}{A_0 + A_S\left(\frac{S}{e^{\tilde{\omega}}}\right)}.$$

The shear-sheltering effect is included through the damping function f_{SS} that can be alternatively defined with different characteristic Reynolds number, as

$$Re_{k\,\Omega} = \frac{k}{\nu\Omega}, \qquad f_{SS} = \exp\left[-\left(C_{SS}\frac{\nu\Omega}{k}\right)^2\right],$$

$$Re_{\sqrt{k}\,d} = \frac{\sqrt{k}d}{\nu}, \qquad f_{SS} = \exp\left[-\left(C_{SS}\frac{\nu}{\sqrt{k}d}\right)^2\right].$$

Kubacky et al. [13] introduced a modification of the model constant C_{SS} to take into account damping or amplification of Klebanoff streaks in accelerating or decelerating flows, for example due to geometry of separation bubbles. In particular

$$C_{SS} = C_S\left(1 + f_k\chi\right), \qquad \chi = tanh\left[\frac{-\Omega\left(S-\Omega\right)}{C_\chi\left(\beta^* e^{\tilde{\omega}}\right)}\right], \qquad f_k = 1 - tanh\left(\frac{\overline{k}}{C_k\nu e^{\tilde{\omega}}}\right), \tag{4}$$

where the C_S, C_χ and C_k are model constants. The effect of acceleration, or deceleration, is taken into account by the χ function, which is positive in accelerating flow due to the curvature, and increases the model constant, thus enlarging the shear sheltering and delaying the transition. The f_k function equals unity near the walls and becomes zero away from walls, and allows to limit the modification of the model constant to the middle part of a pre-transitional boundary layer.

The production term of the turbulent kinetic energy due to separation-induced transition is written as the maximum function between two different contributions to the production of the tubulent kinetic energy, as

$$P_{SI} = \max\left(P_{SI\,1}, P_{SI\,2}\right), \tag{5}$$

$$P_{SI\,1} = \left(1-\gamma\right)\max\left(2.8Tu_\infty\mu - \overline{\mu}_t, 0\right)C_{SI}F_{SI}\mu S^2, \tag{6}$$

$$P_{SI\,2} = C_{Kleb}f_{Kleb}kS, \qquad f_{Kleb} = f_\gamma f_\omega \tag{7}$$

$$Re_{d^2\,S} = \frac{Sd^2}{\nu}, \qquad F_{SI} = \exp\left[-\left(\frac{A_{SI}}{Re_{d^2\,S}}\right)\right] = \exp\left[-\left(A_{SI}\frac{\nu}{Sd^2}\right)\right].$$

$$f_\gamma = \frac{1}{1 + exp\left[b_\gamma\left(\gamma - a_\gamma\right)\right]},$$

$$f_\omega = \frac{1}{1+\exp\left[-b_\omega\left(Re_\omega - a_\omega\right)\right]} = \frac{1}{1+\exp\left[-b_\omega\left(\frac{e^{\tilde{\omega}}d^2}{\nu} - a_\omega\right)\right]},$$

The first term $P_{SI\,1}$ models the breakdown of the separated shear layer due to the Kelvin-Helmholtz instabilities under low freestream turbulent intensity levels, while the second term $P_{SI\,2}$ adjusts the production for moderate and high turbulent intensities. F_{SI} and f_{Kleb} are the detection functions for the separated shear layers to allow the production of the turbulent kinetic energy for the separation-induced mode cases. In comparison with Kubacki et al. [13], where $P_{SI\,1} = \left(1-\gamma\right)C_{SI}F_{SI}\mu S^2$ and $F_{SI} = \min\left[\max\left(Re_{d^2\,S}/\left(2.2A_{SI}\right) - 1, 0\right), 1\right]$, the term here proposed adds an exponential function to increase the smoothness, similarly to the intermittency and the shear-sheltering damping functions. Furthermore, the term $\max\left(2.8Tu_\infty\mu - \overline{\mu}_t\right)$ is

added to limit the production of the turbulent kinetic energy downstream near the reattachment region of the flow, and is similar to the term proposed by Menter et al. [14]. In particular, 3μ is replaced with $2.8Tu_\infty\mu$ to introduce an influence to the freestream turbulent intensity also in the separation-induced transition cases. Without this term, in plates with a blunt leading edge, there is an unphysical creation of turbulence due to normal straining, and this is important for low freestream turbulence intensities, where the turbulent intensity in the separation region shows an over-prediction [7].

The intermittency function is traditionally defined according to the definition of the shear-sheltering function, i.e., to the characteristic Reynolds number used in the shear-sheltering function, as

$$Re_{\sqrt{k}\,d} = \frac{\sqrt{k}d}{\nu}, \qquad \gamma_1^* = \min\left(\max\left(\frac{\sqrt{k}d}{\nu} - C_{TH\,1}, 0\right), 1\right), \tag{8}$$

$$Re_{k\,\Omega} = \frac{k}{\nu\Omega}, \qquad \gamma_2^* = \min\left(\max\left(\frac{k}{\nu\Omega} - C_{TH\,2}, 0\right), 1\right), \tag{9}$$

where C_{TH} is the threshold value of transition. According to Kubacki et al. [13] the intermittency formulation can be based also on the dissipation rate of the turbulent kinetic energy, as

$$Re_{k\omega} = \frac{ke^{\tilde{\omega}_r}}{\nu\Omega^2}, \qquad \gamma_3^* = \min\left(\max\left(\frac{ke^{\tilde{\omega}_r}}{\nu\Omega^2} - C_{TH\,3}, 0\right), 1\right), \tag{10}$$

where an exponential law is here used to improve the smoothness of the intermittency function and the transition, i.e., $\gamma_i = 1 - \exp\left(\gamma_i^*/A_{TH\,i}\right)$. Furthermore, the performance of these formulations of the intermittency function is compared with an alternative formulation from the SA-BCM transition model [9], i.e., from Eqs. (2) and (3), here called γ_4.

Both the production terms of the turbulent kinetic energy and the specific dissipation rate include the intermittency function, differently from the models proposed by Holman and Fürst [7] and Kubacki et al. [13]. In fact, as spotlighted in Lorini et al. [3, 4], the presence of the intermittency in the production term of the specific dissipation rate avoids shorter transition flow regions. The same intermittency function is used for both production terms without any limiter. The intermittency is also activated when a large value of the turbulent kinetic energy appears together with a relatively large value of the distance to the wall, which occurs with a large separation zone caused by a very strong adverse pressure gradient combined with a high freestream turbulence level.

At solid walls the homogeneous Neumann condition for the specific dissipation rate is prescribed and, since the velocity is equal to zero due to the no-slip condition, the turbulent kinetic energy at the wall is also zero, i.e., $k_{wall} = 0$. At inflow or freestream the specific dissipation rate and turbulent kinetic energy values are computed according to the definition of freestream turbulent intensity Tu_∞ and turbulent viscosity ratio $(\mu_T/\mu)_\infty$.

4 ZERO PRESSURE GRADIENT FLAT PLATES

The T3A, T3B and T3A- flat plates of the ERCOFTAC T3 series with zero pressure gradient are here used to validate and calibrate the transition models with bypass transition mode. These cases are characterized by different values of the Reynolds number and turbulence intensity at

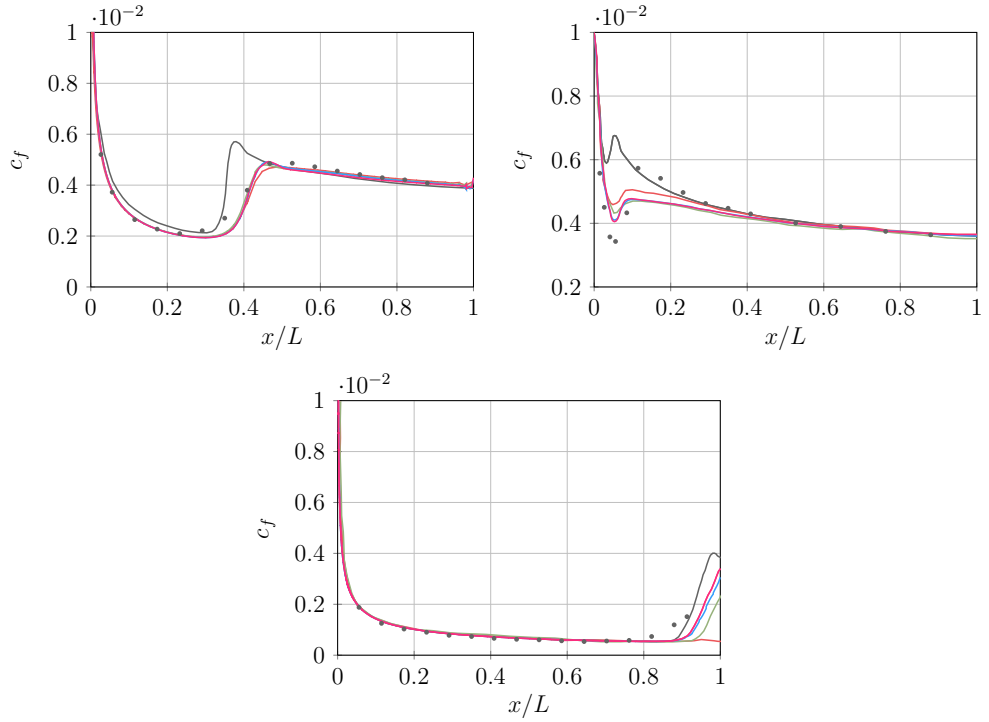

Figure 2: Zero pressure gradient flat plates. Skin friction coefficient c_f along the plate for the zero pressure gradient flat plates, T3A (top,left), T3B (top, right) and T3A- (bottom), with the γk-$\tilde{\omega}$ model, from $\mathbb{P}^1$ to $\mathbb{P}^4$ solution approximation. — $DG-\mathbb{P}^1$, — $DG-\mathbb{P}^2$, — $DG-\mathbb{P}^3$, — $DG-\mathbb{P}^4$, — Holman and Fürst γk-ω, • Coupland exp.

the leading edge. The inlet turbulent quantities of the γk-$\tilde{\omega}$ model, e.g, Tu_∞ and $(\mu_T/\mu)_\infty$, are chosen in order to match the experimental turbulent intensity at the leading edge and the decay of the turbulent intensity along the domain. In particular the turbulence intensity at the leading edge of the plate is $Tu = 3.0\%$ in the T3A case, $Tu = 6.0\%$ in the T3B case, and $Tu = 0.9\%$ in the T3A- case, while the freestream velocity is 5.4, 9.4, and $19.8 m/s$, respectively. The same mesh, made of 8 800 quadrilateral elements with linear edges, is used for all the cases. All the intermittency functions proposed for the γk-$\tilde{\omega}$ model are similar and can be used indiscriminately.

Figures 2 and 3 show the skin friction coefficient distribution on the plates with the γk-$\tilde{\omega}$ model and different solution approximation and with the SA-BCM model and different inlet working variable $\tilde{\nu}_\infty/\nu = 1.5 \times 10^i$ with $i = \{3, \dots, -14\}$. With both the models the solutions show a better prediction of the transition in comparison to Holman and Fürst [7] in every case. The best values of the inlet working variable $\tilde{\nu}_\infty/\nu$ for the T3A and T3B cases are similar of the recommendation by Cakmakcioglu et al. [9], while for the T3A- case the value must be decreased to the limit (1.5×10^{-14}). The motivation of this value, out of the prescribed range, can be found in the very low level of the turbulent intensity, which allows to get closer to a natural transition mode case.

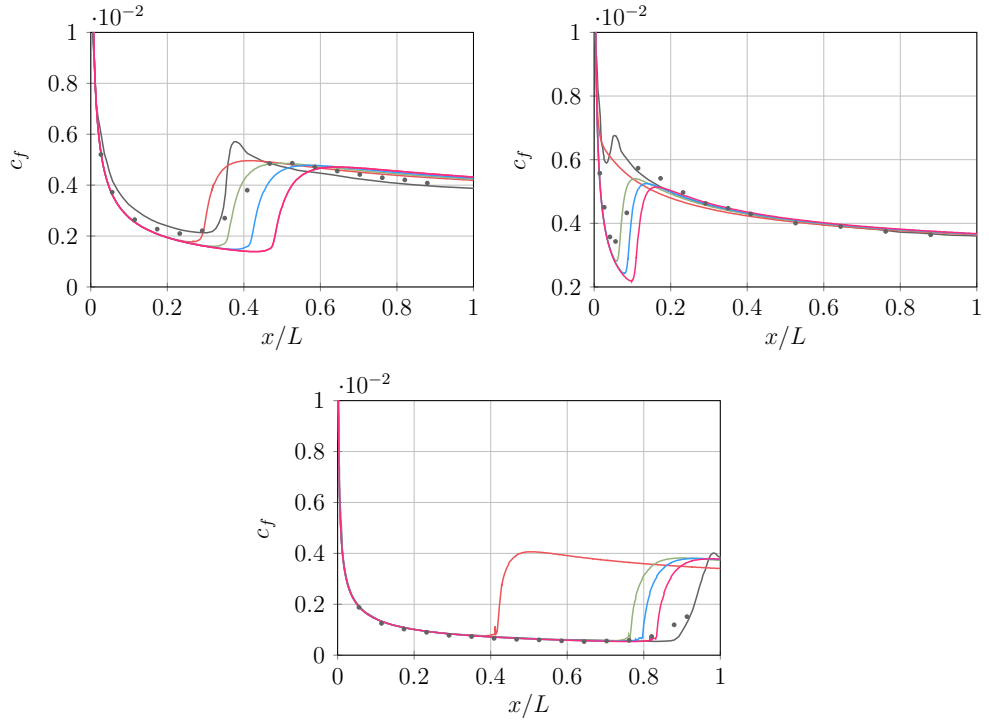

Figure 3: Zero pressure gradient flat plates. Skin friction coefficient c_f along the plate for the zero pressure gradient flat plates, T3A (top,left), T3B (top, right) and T3A- (bottom), with the SA-BCM model and different inlet working variables $\tilde{\nu}_\infty$, $\mathbb{P}^4$ solution approximation. T3A: — $\tilde{\nu}_\infty/\nu = 1.5\times10^{-1}$, — $\tilde{\nu}_\infty/\nu = 1.5\times10^{-2}$, — $\tilde{\nu}_\infty/\nu = 1.5\times10^{-3}$, — $\tilde{\nu}_\infty/\nu = 1.5\times10^{-4}$, T3B: — $\tilde{\nu}_\infty/\nu = 1.5\times10^{0}$, — $\tilde{\nu}_\infty/\nu = 1.5\times10^{-1}$, — $\tilde{\nu}_\infty/\nu = 1.5\times10^{-2}$, — $\tilde{\nu}_\infty/\nu = 1.5\times10^{-3}$, and T3A-: — $\tilde{\nu}_\infty/\nu = 1.5\times10^{-2}$, — $\tilde{\nu}_\infty/\nu = 1.5\times10^{-12}$, — $\tilde{\nu}_\infty/\nu = 1.5\times10^{-13}$, — $\tilde{\nu}_\infty/\nu = 1.5\times10^{-14}$. — Holman and Fürst γk-ω, • Coupland exp.

5 ROUNDED LEADING EDGE FLAT PLATES

The T3L1 and T3L3 rounded leading edge flat plates of the ERCOFTAC T3 series with zero pressure gradient are here used to validate and calibrate the transition models with separation-induced transition mode. These cases are characterized by different values of the Reynolds number and turbulent intensity at the leading edge. The inlet turbulent quantities of the γk-$\tilde{\omega}$ model, e.g, Tu_∞ and $(\mu_T/\mu)_\infty$, are chosen in order to match the experimental turbulent intensity at the leading edge and the decay of the turbulent intensity along the domain. In particular the turbulence intensity at the leading edge of the plate is $Tu = 0.2\%$ in the T3L1 case and $Tu = 2.3\%$ in the T3L3 case, while the freestream Reynolds numbers is $Re_D = 3450$, based on the diameter of the leading edge of the plate and the freestream flow conditions. The same mesh, made of 15 500 quadrilateral elements with quadratic edges, is used for all the testcases.

Figures 4 and 5 show the skin friction coefficient distribution on the plates with the γk-$\tilde{\omega}$ model and different solution approximation and with the SA-BCM model and different inlet working variable $\tilde{\nu}_\infty/\nu = 1.5\times10^{i}$ with $i = \{1,\dots,-2\}$. With both the models the solutions

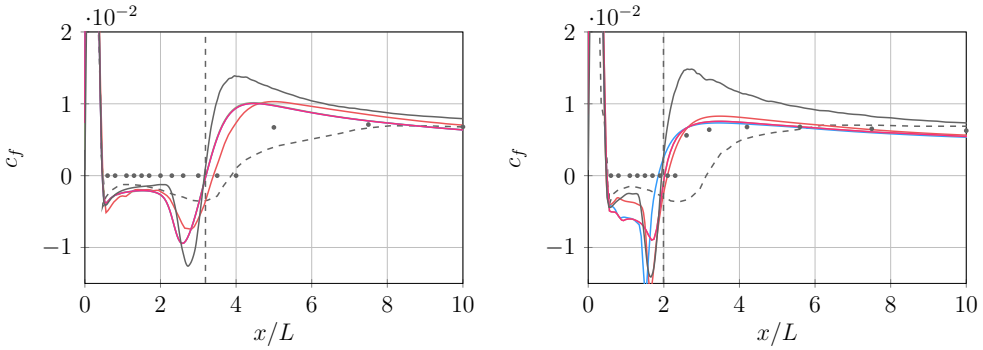

Figure 4: Rounded leading edge flat plates. Skin friction coefficient c_f along the domain for the rounded leading edge flat plates, T3L1 (left) and T3L3 (right), with the γk-$\tilde{\omega}$ model, from $\mathbb{P}^1$ to $\mathbb{P}^4$ solution approximation. The vertical dashed line represent the experimental length of the laminar separation bubble [6]. The references from Vlahostergios et al. [15] are here reported with linear k_L-k-ω model. — $DG-\mathbb{P}^1$, — $DG-\mathbb{P}^2$, — $DG-\mathbb{P}^3$, — $DG-\mathbb{P}^4$, - - - Vlahostergios et al. k_L-k-ω, — Bassi et al. ILES, • Coupland exp.

show a better prediction of the transition in comparison to Vlahostergios et al. [15] in every case. Also on this testsuite, a lower level of the turbulent intensity needs a lower value of the inlet working variable for the SA-BCM model, in fact on the T3L1 case the more accurate solution is with $\tilde{\nu}_\infty/\nu = 1.5 \times 10^{-2}$. The distributions of the skin friction coefficient in the reattached and fully turbulent boundary layer of both the model are in agreement with experiments [6] and the numerical results of Vlahostergios et al. [15], while underestimate the numerical results of Bassi et al. [12]. In fact, the higher skin friction coefficient distribution of the (unsteady) high-fidelity simulations of Bassi et al. [12] is due the the unsteadiness of the flow and in particular to the velocity fluctuations. The (steady) transition models underestimate the distribution of the skin friction coefficient after the reattachment of the boundary layer, due to a natural inability to predict the velocity fluctuations.

6 CONCLUSIONS

The implementation of a modified version of the k-$\tilde{\omega}$ [8] and Spalart-Allmaras [10] turbulence models in a high-order dG solver to predict transition due to the bypass and separation-induced modes is here presented. The modifications of these turbulence models are based on the γk-ω by Holman and Fürst [7] and Kubacki et al. [13], and the SA-BCM by Cakmakcioglu et al. [9]. Both the proposed transition models are correlation-based algebraic transition models that relies on local flow information and include an intermittency function instead of an intermittency equation.

The accuracy of both the transition models is demonstrated in comparison with experiments and numerical results from literature, on different benchmark cases and for increasing order of accuracy. The solutions are in good agreement with the references in all the cases, starting from a sufficient solution approximation, where a good choice of the inlet or freestream working variable for the SA-BCM model is mandatory. In particular cases with a low level of the freestream turbulent intensity need lower values of the working variable at the boundary, which

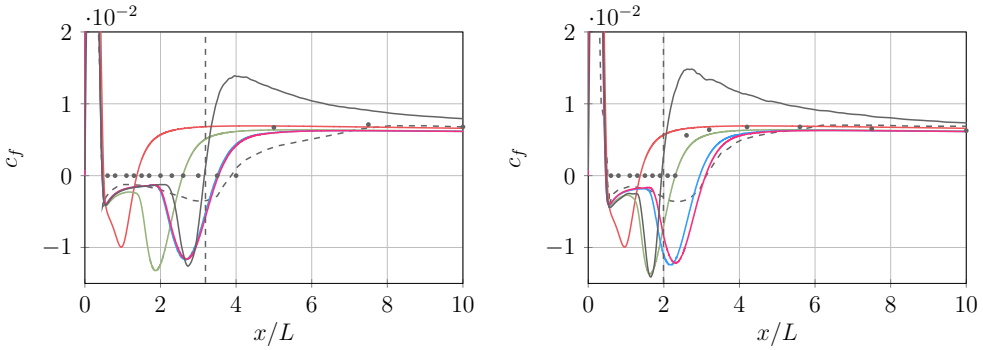

Figure 5: Rounded leading edge flat plates. Skin friction coefficient c_f along the domain for the rounded leading edge flat plates with the SA-BCM model and different inlet working variables $\tilde{\nu}_\infty$, T3L1 (left) and T3L3 (right), $\mathbb{P}^4$ solution approximation. The vertical dashed line represent the experimental length of the laminar separation bubble [6]. The references from Vlahostergios et al. [15] are here reported with linear k_L-k-ω model. — $\tilde{\nu}_{far}/\nu = 1.5 \times 10^1$, — $\tilde{\nu}_{far}/\nu = 1.5 \times 10^0$, — $\tilde{\nu}_{far}/\nu = 1.5 \times 10^{-1}$, — $\tilde{\nu}_{far}/\nu = 1.5 \times 10^{-2}$, - - - Vlahostergios et al. k_L-k-ω, — Bassi et al. ILES, • Coupland exp.

are out of the prescribe range of values [9]. The work is in progress in the application of the models on more complex testcases, as turbine or compressor cascades.

REFERENCES

[1] Bassi, F. and Colombo, A. and Crivellini, A. and Fidkowski, K. J. and Franciolini, M. and Ghidoni, A. and Noventa, G. An entropy-adjoint p-adaptive discontinuous Galerkin method for the under-resolved simulation of turbulent flows. *AIAA Aviation 2019 Forum*, `https://doi.org/10.2514/6.2019-3418` (2019).

[2] Bassi, F. and Colombo, A. and Crivellini, A. and Fidkowski, K.J. and Franciolini, M. and Ghidoni, A. and Noventa, G. Entropy-adjoint p-adaptive discontinuous Galerkin method for the under-resolved simulation of turbulent flows. *AIAA Journal* **58**, `https://doi.org/10.2514/1.J058847` (2020).

[3] Bassi, F. and Colombo, A. and Ghidoni, A. and Lorini, M. and Noventa, G. Discontinuous Galerkin solution of the Reynolds-Averaged Navier-Stokes and $k_L - k_T - \tilde{\omega}$ transition model equations, *ECCOMAS Congress 2016 - Proceedings of the 7th European Congress on Computational Methods in Applied Sciences and Engineering*, `https://doi.org/10.7712/100016.1986.6971` (2016).

[4] Lorini, M. and Bassi, F. and Colombo, A. and Ghidoni, A. and Noventa, G. Discontinuous Galerkin solution of the RANS and $k_L - k_T - \tilde{\omega}$ equations for natural and bypass transition, *Computers and Fluids* **214**, `https://doi.org/10.1016/j.compfluid.2020.104767` (2021).

[5] Noventa, G. and Massa, F. and Rebay, S. and Bassi, F. and Ghidoni, A. Robustness and efficiency of an implicit time-adaptive discontinuous Galerkin solver for unsteady flows. *Computers and Fluids* **204**, https://doi.org/10.1016/j.compfluid.2020.104529 (2020).

[6] Coupland, J. ERCOFTAC Special Interest Group on Laminar to Turbulent Transition and Retransition: T3A and T3B test cases, Technical Report (1990).

[7] Holman, J. and Fürst, J. Coupling the algebraic model of bypass transition with EARSM model of turbulence, *Advances in Computational Mathematics* **45**, https://doi.org/10.1007/s10444-019-09680-2 (2019).

[8] Bassi, F. et al. Time integration in the discontinuous Galerkin code MIGALE - steady problems, Notes on Numerical Fluid Mechanics and Multidisciplinary Design, *Springer International Publishing* (2015).

[9] Cakmakcioglu, S. C. and Bas, O. and Mura, R. and Kaynak, U. A Revised One-Equation Transitional Model for External Aerodynamics, *AIAA Aviation 2020 Forum*, https://doi.org/10.2514/6.2020-2706 (2020).

[10] Crivellini, A. and D'Alessandro, V. and Bassi, F. A Spalart-Allmaras turbulence model implementation in a discontinuous Galerkin solver for incompressible flows, *Journal of Computational Physics* **241**, https://doi.org/10.1016/j.jcp.2012.12.038 (2013).

[11] Colombo, A. and Ghidoni, A. and Noventa, G. and Rebay, S. p-Multigrid High-Order Discontinuous Galerkin Solution of Compressible Flows, *CISM International Centre for Mechanical Sciences*, https://doi.org/10.1007/978-3-030-60610-7_4 (2021).

[12] Bassi, F. et al. A p-adaptive Matrix-Free Discontinuous Galerkin Method for the Implicit LES of Incompressible Transitional Flows, *Flow, Turbulence and Combustion* **105**, https://doi.org/10.1007/s10494-020-00178-2 (2020).

[13] Kubacki, S. et al. Extension of an algebraic intermittency model for better prediction of transition in separated layers under strong free-stream turbulence, *International Journal of Heat and Fluid Flow* **92**, https://doi.org/10.1016/j.ijheatfluidflow.2021.108860 (2021).

[14] Langtry, R. B. et al. A Correlation-Based Transition Model Using Local Variables - Part II: Test Cases and Industrial Applications, *Journal of Turbomachinery* **128**, https://doi.org/10.1115/1.2184353 (2004).

[15] Vlahostergios, Z. and Yakinthos, K. and Goulas, A. Separation-induced boundary layer transition: Modeling with a non-linear eddy-viscosity model coupled with the laminar kinetic energy equation, *International Journal of Heat and Fluid Flow* **30**, https://doi.org/10.1016/j.ijheatfluidflow.2009.02.004 (2009).

[16] Spalart, P. R. and Garbaruk, A. G. Correction to the Spalart–Allmaras Turbulence Model, Providing More Accurate Skin Friction, *AIAA Journal* **58**, https://doi.org/10.2514/1.J059489 (2020).